Detection and Classification of the Broken Rotor Bars in Squirrel-Cage Induction Motors

Abdurrahman Ünsal, Özkan Kara

Abstract— **Mechanical faults, stator faults and rotor faults are the major faults of induction motors. Rotor faults constitute about 10% of total faults of induction motors. The main reasons of rotor faults are the broken rotor bars. Many methods have been used to detect broken rotor bars till now. In this paper, a new method is introduced. A squirrel-cage induction motor is modeled by using MATLAB/Simulink. Model takes motor speed as an input and finds the frequency of side-band harmonics of stator current. Then model compares the magnitudes of side-band harmonics with the magnitude of fundamental component and classifies them according to the number of broken rotor bars. At any load and speed, the method can find and classify the broken rotor bars based on the number of broken rotor bars. Experimental results, along with simulation results verifies the effectiveness of the method.**

Index Terms— **Broken rotor bars, detection, induction motors, simulation.**

I. Introduction

Induction motors are the major motors used mainly in industry. Therefore it is very important to use motors with minimum fault. Any fault (related to induction motors) takes place in industry may result in significant downtime and financial losses. Stator faults, mechanical faults, and rotor faults can be counted as the major faults of induction motors. Stator faults caused by short-circuited coil or weak insulation. Rise in temperature and vibration occurs in induction motor as a result of stator faults. Mechanical faults are mainly originated from bearing and misalignment faults. Vibration occurs as a result of mechanical faults. Rotor faults especially result from broken rotor bars. Rotor faults cause harmonics in stator current, vibration and temperature rise. According to the results of latest fault surveys approximately 38% of the total faults of induction motor are due to stator faults, 40% of the total faults are due to mechanical faults, 10% of the total faults due to rotor faults and 12% of the total faults are due to other mechanical faults [1].

Stator current, voltage, noise, heat, torque, and vibration signals are mostly used to detect induction motor faults. Motor current signature analysis (MCSA) is a commonly used method to detect rotor faults by observing side-band harmonic frequencies of stator current [2-3]. Time domain analysis and frequency domain analysis are the main methods for MCSA. The side-band harmonic frequencies of stator current can also be used to diagnose broken rotor bars for large motors [4].

Manuscript received June 08, 2016

Abdurrahman ÜNSAL, Electrical and Electronics Engineering, Dumlupinar University, Kütahya, Turkey

Özkan KARA, Electrical and Electronics Engineering, Sakarya University, Sakarya, Turkey

When there is a broken rotor bar, induction motor heats more than induction motor with healthy rotor. It may also vibrates compared to the healthy motor. Therefore its noise is more than the healthy motor. Frequency signal dimension order estimator can be created to compare faulty and healthy rotors and decide on the healthiness of the rotor [5]. By using wavelet analysis and by observing heat, torque, noise and vibration signals, rotor faults can also be detected [6-7]. Startup transient currents may be observed by using wavelet method. In this method it is not necessary to load the induction motor for fault detection [8-9].

Digital signal processing method is another method to diagnose rotor faults [10-11-12]. To achieve success in this method, the signal should have harmonic sinusoids. The rotor faults can be diagnosed by monitoring the signatures of current, voltage, heat and vibration signals. This method is also used for condition monitoring of induction motors [13-14]. By measuring vibration signals and observing frequency features, rotor faults can also be detected [15-16]. In global fault index method, stator current besides stator voltage is measured and then the power of the induction motor is calculated. Broken rotor bars are detected by using periodograms such as Bartlett periodogram [17]. Comparison of power spectrum with the stator current is another way to detect rotor faults [18-19]. With instantaneous power spectrum, it possible to detect broken rotor bars even at low slips [20]. Flux analysis uses magnetic flux density to diagnose rotor faults (mainly used for large motors) [21].

Stator current analysis is the most commonly used method to detect rotor faults. Broken rotor bar is the main reason of the rotor faults. When there is a broken rotor bar in the induction motor, side-band harmonic frequencies (f_b) appear at both sides of fundamental frequency of stator current. Side-band harmonic frequencies can be found as:

$$f_b = (1 \pm 2ks) f_1, \quad \text{k= 1, 2, 3} \qquad (1)$$

where 'f_b' represents side-band harmonic frequencies, 's' represents slip and 'f_1' represents fundamental component frequency.

As load of the induction motor increases, slip also increase. Therefore side-band harmonic frequency changes and as slip increase side-band harmonic frequency diverges from the fundamental component frequency. Closeness of the side-band harmonic frequency to the fundamental component frequency at 25% loading condition is more than the closeness of the side-band harmonic frequency to the fundamental component frequency at 100% loading condition. Not only closeness of the side-band harmonic frequency to the fundamental component frequency changes but also the magnitudes of the side-band harmonics change

with the loading of the motor. Magnitudes of the side-band harmonics at 100% loading are bigger than the magnitudes of the side-band harmonics at 25% loading. At the same loading condition; the magnitudes of the side-band harmonics also increase as the number of broken rotor bar increases [22]. This condition can be formulated as:

$$\frac{I_{bb}}{I} = \frac{n_{bb}}{N_b} \tag{2}$$

where 'I_{bb}' represents the magnitude of side-band harmonics, 'I' represents the magnitude of fundamental component, 'n_{bb}' represents the number of broken rotor bars and 'N_b' represents the total number of rotor bars.

The resistance of rotor increases as the number of broken rotor bars increase [23-24]. The change in the resistance of the rotor can be written as

$$\Delta r_r = r_r \frac{3n_{bb}}{N_b - 3n_{bb}} \tag{3}$$

where 'Δr_r' represents the change in rotor resistance for each phase, 'r_r' represents rotor resistance for each phase.

In this paper, a squirrel-cage induction motor is modeled by using MATLAB/Simulink. Model takes motor speed as an input and finds the frequency of side-band harmonics. Then model compares the magnitudes of side-band harmonics with the magnitude of fundamental component of stator current and classifies them according to the number of broken bars. At any load and speed, the method can find and classify the number of broken rotor bars. In the study, Simulink model will be introduced first. Then, simulation results will be presented. Finally, experimental results will be presented and compared with the simulation results.

II. Mathematical Model of The Induction Motor

Equations of rotor and stator are deduced according to dq frame. As a matter of convenience three-axis frame (abc frame) translated into two-axis reference frame (dq frame) as follows [25-26];

Q -Axis Model;

$$R_s I_{qs} + (L_s - \frac{L_m^2}{L_r})\frac{dI_{qs}}{dt} = V_{qs} - \frac{L_m}{L_r}\frac{d\varphi_{qr}}{dt} \tag{4}$$

$$\frac{L_r}{R_r}\frac{d\varphi_{qr}}{dt} + \varphi_{qr} = I_{qs}L_m + \frac{L_r}{R_r}(\omega\frac{P}{2})\varphi_{dr} \tag{5}$$

D-Axis Model;

$$R_s I_{ds} + (L_s - \frac{L_m^2}{L_r})\frac{dI_{ds}}{dt} = V_{ds} - \frac{L_m}{L_r}\frac{d\varphi_{dr}}{dt} \tag{6}$$

$$\frac{L_r}{R_r}\frac{d\varphi_{dr}}{dt} + \varphi_{dr} = I_{ds}L_m - \frac{L_r}{R_r}(\omega\frac{P}{2})\varphi_{qr} \tag{7}$$

Slip;

$$s = \frac{\frac{200\pi}{P} - \omega}{\frac{200\pi}{P}} \tag{8}$$

Load and Speed;

$$T_e = \frac{3}{2}\frac{P}{2}\frac{L_m}{L_r}(\varphi_{dr}I_{qs} - \varphi_{qr}I_{ds}) \tag{9}$$

$$T_{damp} = F\omega \tag{10}$$

$$J\frac{d\omega}{dt} = T_e - T - T_{damp} \tag{11}$$

Side-band harmonic frequencies are found by using motor speed as follows;

$$f_b = (1 \pm 2\frac{\frac{200\pi}{P} - \omega}{\frac{200\pi}{P}})f_1 \tag{12}$$

where R_s, R_r are the stator and rotor resistances; L_s , L_r , L_m are stator, rotor and mutual inductances; V_{qs}, V_{ds} are q and d axis stator voltages; I_{qs} , I_{ds} are q and d axis stator currents; φ_{qr} , φ_{dr} are rotor q and d axis fluxes; ω is the rotor angular speed; P is pole pair; T is load torque; T_e electromagnetic torque; T_{damp} is the damping torque; J is rotor and load inertia; F is the rotor and load friction coefficient; f_1 is the fundamental component frequency; f_b is the side-band harmonic frequency; s is slip; n_{bb} is the number of broken rotor bars, and N_b is number of total rotor bars.

III. Simulink Model

The Simulink model is developed according to equations 1-12. In the simulation model, user can set the loading of the motor and the number of broken rotor bars from the menu. The loading can be selected as 25% load, 50% load, 75% load and 100%. The nameplate parameters of three-phase induction motor used in the model are: 7.5 kW; 380 V-50 Hz; 2850 rpm, 2 poles, 30 rotor bars. User can enter parameters of the induction motor from the functional block of the model.

Apart from the model used in the previous work [26]; this model uses total number of rotor bars to classify the rotor fault according to number of broken rotor bars as in equation (2), side-band harmonics are calculated in the same block (see Fig. 1), change in rotor resistance is calculated according to equation (3), motor speed is used to find the frequency of side-band harmonics. Details of the model is given in Figure 1.

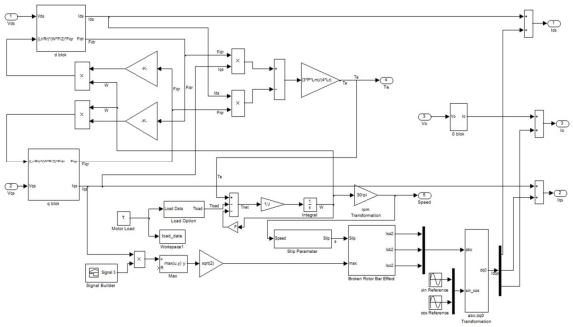

Figure 1. Details of the parameter computation block

IV. Simulation Results

The developed model was tested under four different loading conditions (25% load, 50% load, 75% load and 100% load) and with two different rotor faults (one broken rotor bar and three broken rotor bars). Under all loading conditions, the induction motor was tested first with healthy rotor, then with one bar broken rotor bar, and then with three broken rotor bars. All stator currents shown in the paper are provided in frequency domain. Due to the limited space in the paper the results of all implemented tests are not provided in this paper. There are no side-band harmonics under all loading conditions when the rotor is healthy. This can be seen from Figure 2.

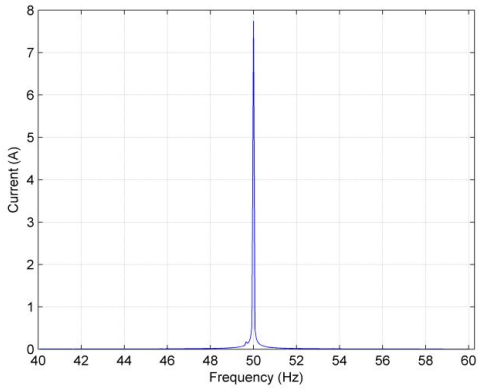

Figure 2. Stator current under 50% loading with healthy rotor

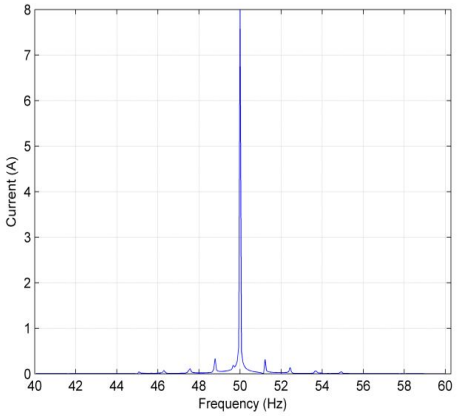

Figure 3. Stator current (with one broken rotor bar) under 50% loading

The motor with one broken rotor bar was first tested under 25% loading. Under this condition side-band harmonic are close the fundamental component of the stator current. The magnitudes of the side-band harmonics are quite low. The second test of the motor with one broken rotor bar was implemented under 50% loading. Figure 3 shows the stator current of the motor with one broken rotor bar under 50% loading. Side-band harmonics are clearly separated from the fundamental component. The magnitudes of the side-band harmonics are medium.

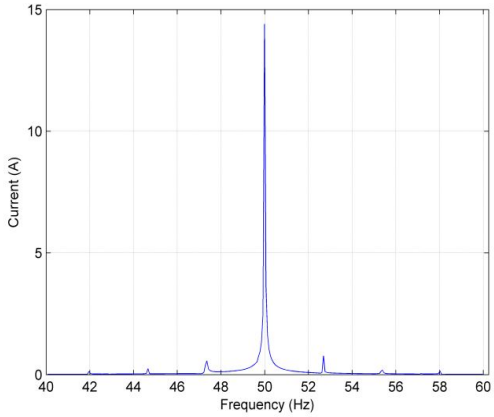

Figure 4. Stator current (with one broken rotor) bar under 100% loading

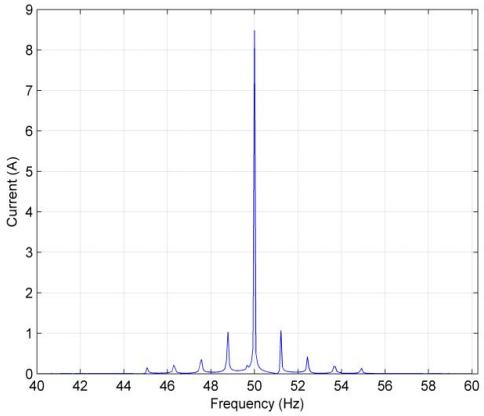

Figure 5. Stator current (with three broken rotor bars) under 50% loading

The third test of the induction motor with three broken rotor bars was implemented under 75% loading. Side-band harmonics are far away from the fundamental component. The magnitudes of the side-band harmonics are higher. The last test was implemented under 100% loading. Figure 4 shows the stator current of the motor with one broken rotor bar under 100% loading. Side-band harmonics are much far away from the fundamental component. The magnitudes of the side-band harmonics are highest. The stator current of motor with three broken rotor bars under 50% loading is shown in Figure 5. The side-band harmonics are clearly seen. Under all loading conditions; as the number of broken rotor bars increases, the magnitudes of the side-band harmonics also increase. Figure 6 indicates the stator current of motor with three broken rotor bars under 100% loading.

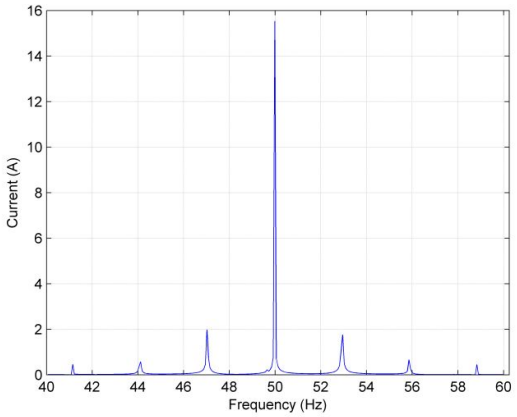

Figure 6. Stator current (with three broken rotor bars) under 100% loading

V. Experimental Results

Experimental set-up is shown in Figure 7. Rotor faults were created by drilling holes on the rotor bars. The motor was loaded with a three phase synchronous generator (which is loaded with a resistive load bank). The loading conditions of the motor were observed from the stator current.

Figure 7. Experimental set-up

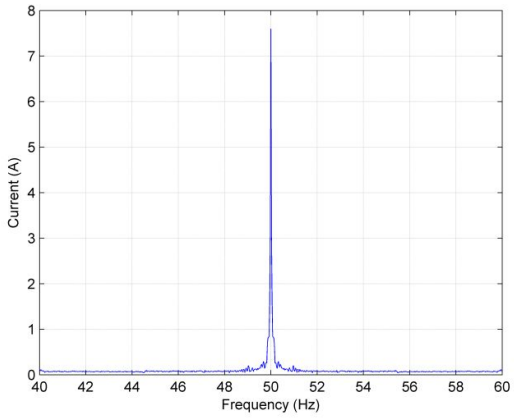

Figure 8. Stator current under 50% loading with healthy rotor

The stator currents of the motor under all loading conditions were recorded by a current transformer and A/D converter. The data of the stator current was converted into excel file by using the software tool provided by Labview. Motor speed data were transfered to another computer by a tachometer. Induction motor was tested under the same rotor faults and loading conditions with the same parameters which was used in the simulation. Broken rotor bars were detected with the developed of software. This software uses motor speed and stator current as inputs for the detection. The results are shown in Figures 8-12. There are no side-band harmonics under all loading conditions when the rotor is healthy (Figure 8).

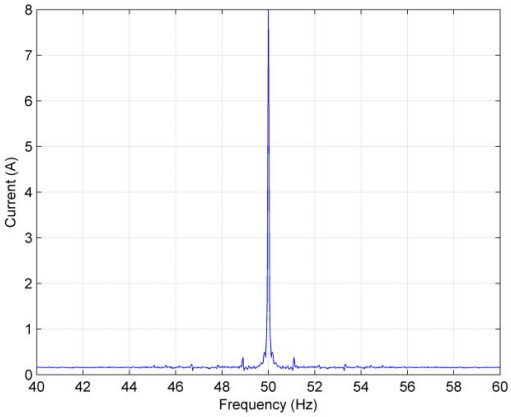

Figure 9. Stator current (with one broken rotor bar) under 50% loading

Under all loading conditions; as the number of broken rotor bars increases, the magnitudes of the side-band harmonics also increase. The induction motor with one broken rotor bar was first tested under 25% loading. The second test was implemented under 50% loading. The last test was implemented under 100% loading. It can be seen from Figure 9 that the side-band harmonics are clearly separated from the fundamental component when the number of rotor bars is one. The magnitudes of the side-band harmonics are medium.

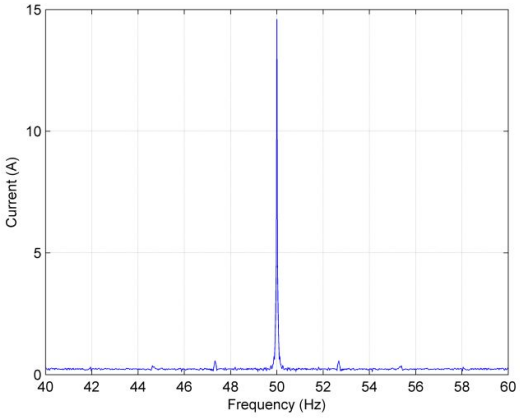

Figure 10. Stator current (with one broken rotor bar) under 100% loading

The side-band harmonics can be clearly seen in Figure 10. It is seen in Figure 11 that side-band harmonics are much far away from the fundamental component when the number of broken rotor bars is three. The magnitudes of the side-band harmonics are highest (Figure 11). The side-band harmonics are clearly seen in Figure 12 since the load and the number of

broken rotor bars are increased. At all loading conditions and broken rotor bar numbers, broken rotor bars are detected and classified according to broken rotor bar numbers successfully.

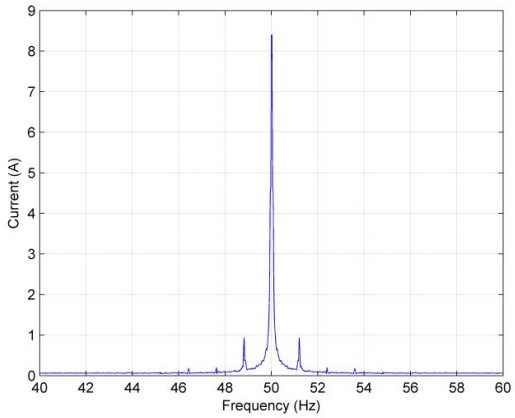

Figure 11. Stator current (with three broken rotor bars) under 50% loading

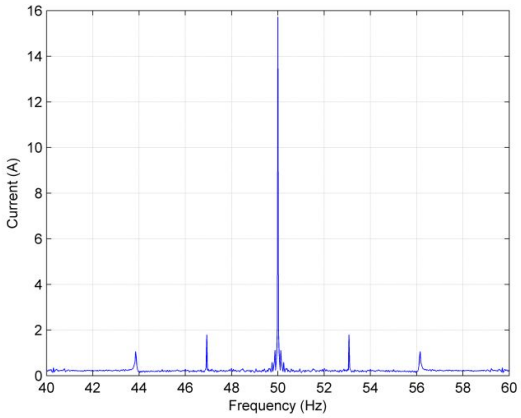

Figure 12. Stator current (with three broken rotor bars) under 100% loading

VI. Comparison of Simulation and Experimental Results

Side-band harmonic frequencies are found by using equation (12). Side-band harmonic frequencies of the test results of motor with one broken rotor bar are presented in Table 1.

Table 1. Side-band harmonic frequencies with one broken rotor bar

Side-band harmonic frequency for one broken rotor bar				
Load (T)	Left S.B.H.F. (Hz)		Right S.B.H.F. (Hz)	
	Simulation	Experimental	Simulation	Experimental
25%	49.29	49.38	50.71	50.62
50%	48.8	48.84	51.2	51.16
75%	48.1	48.12	51.9	51.88
100%	47.4	47.38	52.6	52.62

Side-band harmonic frequencies of the test results of motor with three broken rotor bar are presented in Table 2.

Side-band harmonics' amplitude versus amplitude of the fundamental component with one broken rotor bar is calculated according to (2) and presented in Table 3. n_{bb}/N_b= 1/30 = 0.033; with one broken rotor bar and n_{bb}/N_b= 2/30 = 0.067; with two broken rotor bars. Therefore; calculated values are: $0.033 \le n_{bb} / N_b \le 0.067$ and $0.033 \le I_{bb} / I \le 0.067$.

The amplitude of side-band harmonics' versus amplitude of fundamental frequency with three broken rotor bars is calculated according to (2) and presented in Table 4. n_{bb}/N_b= 3/30 = 0.1; with three broken rotor bars and n_{bb}/N_b= 4/30 = 1.134; with four broken rotor bars. Therefore; calculated values are: $0.1 \le n_{bb} / N_b \le 0.134$ and $0.1 \le I_{bb} / I \le 0.134$.

Table 2.Side-band harmonic frequencies with three broken rotor bars

Side-band harmonic frequencies for three broken rotor bar				
Load (T)	Left S.B.H.F. (Hz)		Right S.B.H.F. (Hz)	
	Simulation	Experimental	Simulation	Experimental
25%	49.28	49.37	50.72	50.63
50%	48.74	48.78	51.26	51.22
75%	47.93	47.95	52.07	52.05
100%	46.87	47	53.13	53

As it is shown in Tables 1-4, experimental results and simulation results are in agreement with each other. In both simulation and experiment results, broken rotor bars are detected and classified according to the number of broken rotor bars. Therefore the performance of the developed model was verified successfully.

Table 3. The amplitude of side-band harmonics e versus the amplitude of fundamental component with one broken rotor bar

I_{bb} / I		
Load (T)	Simulation	Experimental
25%	0.19/5.6 = **0.0339**	0.21/5.58 = **0.0376**
50%	0.33/7.99 = **0.0413**	0.38/8 = **0.0475**
75%	0.75/11.6 = **0.0646**	0.47/11.5 = **0.0408**
100%	0.57/14.4 = **0.0395**	0.576/14.6 = **0.0394**

Table 4. The amplitude of side-band harmonics versus the amplitude of fundamental component with three broken rotor bars

I_{bb} / I		
Load (T)	Simulation	Experimental
25%	0.59/5.86 = **0.1007**	0.77/5.85 = **0.131**
50%	1.03/8.48 = **0.121**	0.935/8.4 = **0.1116**
75%	1.45/12.42 = **0.116**	1.314/12.4 = **0.1059**

100%	2/15.53 = **0.1287**	1.8/15.72 = **0.1145**

CONCLUSION

In this paper, broken rotor bars in a squirrel-cage induction motor are analyzed, detected and classified. Bu using Simulink, simulation model is modeled. The model was tested under four loading conditions (25%, 50%, 75%, 100%) with one and three broken rotor bars. An induction motor was tested under the same rotor faults and loading conditions with the same parameters which was used in the simulation. The experimental results and simulation results are in agreement with each other and with those in the literature. In both simulation and experimental results, the method found and classified the broken rotor bars according to their numbers at any load and speed. The model can be successfully used for educational purposed to detect the broken rotor bars.

REFERENCES

[1] Sin ML, Soong WL, Ertugrul N. Induction machine on-line condition monitoring and fault diagnosis – a survey. In: AUPEC2003 Australasian Universities Power Engineering Conference;28 September-1 October 2003; Christchurch, New Zealand. pp. 1-18.

[2] Neelam M, Ratna D. Motor current cignature analysis and its applications in induction motor fault diagnosis. Int J Syst Ap, Eng & Dev 2007; 2: 442-448.

[3] Benbouzid MH. A review of induction motors signature analysis as a medium for faults detection. IEEE T Ind Electron 2000; 47: 984-993.

[4] Faiz J, Ebrahimi BM. A new pattern for detecting broken rotor bars in ınduction motors during start-up. IEEE T Magn 2008; 44: 4673-4683.

[5] Hwang DH, Youn YW, Sun JH, Kim YH. Robust diagnosis algorithm for identifying broken rotor bar faults in ınduction motors. J Electr Eng & Technol 2014; 9: 37-44.

[6] Nandi S, Toliyat HA, Li X. Condition monitoring and fault diagnosis of electrical motors - a review. IEEE T Energy Conver 2005; 20: 719-729.

[7] Basak D, Tiwari A, Das SP. Fault diagnosis and condition monitoring of electrical machines - A Review. In:ICIT IEEE International Conference on Industrial Technology; 15-17 December 2006; Mumbai, India. New York, NY, USA: IEEE.pp. 3061-3066.

[8] Douglas H, Pillay P, Ziarani A. Detection of broken rotor bars in induction motors using wavelet analysis. In: IEMDC IEEE International Electric Machines and Drives Conference;1-4 June 2003; Madison, Wisconsin, USA.New York, NY, USA: IEEE.pp. 923-928.

[9] Siddiqui KM, Giri VK. Broken rotor bar fault detection in ınduction motors using transient current analysis. Int J Electron & CommunTechnol 2011; 2: 114-119.

[10] Kia SH, Henao H, Capolino GA. Digital signal processing for induction machines diagnosis - a review. In:The 33rd Annual Conference of the IEEE Industrial Electronics Society (IECON); 5-8 November 2007; Taipei, Taiwan. New York, NY, USA: IEEE. pp.1155-1162.

[11] Bellini A, Filippetti F, Tassoni C,Capolino G. Advances in diagnostic techniques for induction machines. IEEE T Ind Electron 2008; 55: 4109-4126.

[12] Matić D, Kanović Ž, Kulić F, Reljić D, Oros Đ, Vasić V. Induction motor broken bar detection for a thermal power-plant application - a case study. ElectrotechVestn 2013; 80:45-49.

[13] Tavner PJ. Review of condition monitoring of rotating electrical machines. IET Electr Power App 2008; 2: 215–247.

[14] Mehala N, Dahiya R. Condition monitoring methods, failure identification and analysis for induction machines. Int J Circ Syst Signal Process 2009; 3: 10-17.

[15] Kanovic Z, Matic D, Jelicic Z, Rapaic M, Jakovljevic B, Kapetina M. Induction motor broken rotor bar detection using vibration analysis — a case study.In: 9th IEEE International Symposium on Diagnostics for Electric Machines Power Electronics and Drives(SDEMPED); 27-30 August 2013; Valencia, Spain.New York, NY, USA: IEEE.pp. 64 – 68.

[16] Jakovljevic BB, Kanovic ZS,Jelicic ZD. Induction motor broken bar detection using vibration signal analysis, principal component analysis and linear discriminant analysis.In: IEEE International Conference on Control Applications (CCA); 3-5 October 2012; Dubrovnik, Croatia.New York, NY, USA: IEEE.pp. 1686 – 1690.

[17] Didier G, Ternisien E, Caspary O, Razik H. Fault detection of broken rotor bars in induction motor using a global fault index. IEEE T Ind Appl 2006; 42: 79 – 88.

[18] Legowski SF, Sadrul Ula AHM, Trzynadlowski AM. Instantaneous power as a medium for the signature analysis of induction motors. IEEE T Ind Appl 1996; 32: 904–909.

[19] Trzynadlowski AM, Ritchie E. Comparative investigation of diagnosis media for induction motor: a case of rotor cage faults. IEEE T Ind Electron 2000; 47:1092–1099.

[20] Maouche Y, Oumaamar MEK, Boucherma M, Khezzar A. A new approach for broken bar fault detection in three-phase induction motor using instantaneous power monitoring under low slip range. Int J Elec & Comput Eng 2014; 4: 52-63.

[21] Dias CG, Chabu IE. Analysis of broken rotor bars in large induction motors. Exacta 2006; 4:333-341.

[22] Chen S. Induction Machine Broken Rotor Bar Diagnostics Using Prony Analysis. MSc,Adelaide University, Adelaide, Australia, 2008.

[23] Chen S, Zivanovic R. Modelling and simulation of stator and rotor fault conditions in induction machine for testing fault diagnostic techniques. EUR T Electr Power 2010; 20:611–629.

[24] Kumar S, Prakash J, Kumar SS. Detection of broken rotor bars in induction motors using derivative free kalman filters.In: International Conference on Process Automation Control and Computing (PACC); 20-22 July 2011; Coimbatore, Tamilnadu, India. New York, NY, USA: IEEE.pp. 1-7.

[25] Baccarini LMR, Menezes BR, Caminhas WM. Fault induction dynamic model, suitable for computer simulation: simulation results and experimental validation. Mech Syst Signal Pr 2010; 24: 300-311.

[26] Unsal A, Kara O. Modelling of broken rotor bars in a squirrel-cage induction motor.In: Forth International Conference on Power Engineering; 13-17 May 2013; Istanbul, Turkey. New York, NY, USA: IEEE.pp. 1597-1602.

Abdurrahman Ünsal (Assoc Prof, PhD) received the BS degree in electrical education from Gazi University, Turkey, in 1992, MS degree in power systems from Oklahoma State University, USA, in 1996, and Ph.D. degree in power systems from Oregon State University, USA, in 2001. He worked with the Department of Electrical and Electronics Engineering, Dumlupinar University, Turkey, from 2002 to 2013 as Assistant Professor. He has been working with the same department as Associate Professor since 2013. His main research interest include electrical machines, fault detection, power quality, and renewable power systems. He is IEEE member since 1998.

Özkan Kara received the BS degree in department of Electrical & Electronics Engineering from Bilkent University, Ankara, Turkey in 2002. He has received the MS degree in department of Electrical & Electronics Engineering from Dumlupınar University, Kütahya, Turkey in 2011. Currently working as an group chief engineer at Turkish Electricity Transmission Company in Kütahya, Turkey and attending PhD study at Electrical Engineering Department in Sakarya University. His interests are basically in Electric Power System Analysis, Stability Analysis in Power Systems, electrical machines, fault detection, power quality.